

Enhanced magneto-optical response due to the flat band in nanoribbons made from the $\alpha - T_3$ lattice

Yan-Ru Chen^{1,2}, Yong Xu², Jun Wang³, Jun-Feng Liu^{1,2,*} and Zhongshui Ma^{4,5†}

¹*Department of Physics, School of Physics and Electronic Engineering, Guangzhou University, Guangzhou 510006, China*

²*Department of Physics, Southern University of Science and Technology, Shenzhen 518055, China*

³*Department of Physics, Southeast University, Nanjing 210096, China*

⁴*School of Physics, Peking University, Beijing 100871, China and*

⁵*Collaborative Innovation Center of Quantum Matter, Beijing, 100871, China*

We study the optical response of nanoribbons made from the $\alpha - T_3$ lattice under a weak magnetic field in the terahertz to far-infrared regime. It is found that the magnetic field can open a gap in the band structure and induce a new absorption peak with much reduced frequency in metallic armchair ribbons and a class of zigzag ribbons with particular boundaries. This tunable magneto-optical modulation effect is attributed to the interband transitions between the flat band and the propagating bands. By contrast, this magnetic modulation of gap opening and optical conductance is much weaker in metallic armchair graphene ribbons (the case of $\alpha = 0$) in which the flat band is absent. The enhancement in the $\alpha - T_3$ model is analytically investigated and explained within the perturbation theory for metallic armchair ribbons. The magnetic field induced valley degeneracy lifting and valley splitting of the absorption peak are also discussed in the case of zigzag ribbons. These findings pave the way for magneto-optics devices based on the $\alpha - T_3$ model materials.

I. INTRODUCTION

Graphene, as a two-dimensional sheet of carbon atoms arranged on a honeycomb lattice, has achieved a great success in both fundamental physics and applications due to its exotic electronic properties¹⁻³. Recently, a modified lattice – the $\alpha - T_3$ lattice, is attracting more and more attention as an interpolation between the honeycomb lattice of graphene and the dice lattice. As shown in Fig. 1(a), the dice or T_3 lattice is obtained by coupling one of the two inequivalent sites of the honeycomb lattice to an additional atom located at the center of each hexagon⁴⁻⁶. The dice lattice could be experimentally realized by growing a trilayer structure of cubic lattices such as SrTiO₃/SrIrO₃/SrTiO₃ in the (111) direction⁷ or by confining cold atoms to an optical lattice⁸. The low-energy quasiparticle in the dice lattice is described by the pseudospin-1 Dirac-Weyl equation^{6,8}. The spectrum contains a pair of linear Dirac cones and an additional dispersionless flat band that cuts through the Dirac points (see Fig. 1(b)). The $\alpha - T_3$ lattice interpolates between graphene ($\alpha = 0$) and the dice lattice ($\alpha = 1$) via a parameter α that describes the strength of the coupling between the honeycomb lattice and the central hub site. Recently, a 2D model for Hg_{1-x}Cd_xTe at critical doping has been shown to map onto the $\alpha - T_3$ model with an intermediate parameter $\alpha = 1/\sqrt{3}$ ⁹. The $\alpha - T_3$ model has also been generalized to include additional terms and variations in its Hamiltonian¹⁰. And the properties of general pseudospin S lattices have also been extensively studied^{6,11,12}.

The α -dependent Berry phase¹³⁻¹⁵ in the $\alpha - T_3$ model results in unusual electronic properties such as unconventional quantum Hall effect^{16,17}, super-Klein tunneling¹⁸⁻²¹, minimal conductivity¹⁴, orbital magnetic response¹³, Weiss oscillations²² etc. Additionally, the

flat band also plays an important role in the transport. Although the flat band itself has zero conductivity due to the zero group velocity, the interplay between the flat band and the propagating bands is predicted to induce a diverging dc conductivity in the presence of disorders²³, or enhance the resulting current in a nonequilibrium situation²⁴. Additionally, the flat band have also attracted much attention for its nontrivial topology²⁵⁻³¹ and interaction effect²⁸⁻³². It is noticeable that the first-principles calculations implied that the flat band can exist in a realistic material²⁵⁻²⁷.

The optical and magneto-optical spectroscopy can be used to probe the underlying electronic structure and as well as design optoelectronic devices. For graphene, the optical and magneto-optical conductivities have been extensively studied for both infinite sheet³³ and nanoribbon geometry³⁴⁻⁴⁰. The optical response at selective frequencies can be enhanced with the use of nanoribbons in graphene. For the $\alpha - T_3$ lattice, the optical⁴¹ and magneto-optical conductivities^{11,42,43} have been studied for infinite sheet. But the optical conductance of nanoribbons from the $\alpha - T_3$ lattice (see Figs. 1(c) and 1(d)) has not been investigated. The effect of a perpendicular magnetic field on the electronic structure and optical conductance of $\alpha - T_3$ nanoribbons is also untouched. It has been shown that the magnetic field can open a gap and induce an absorption peak in metallic armchair graphene nanoribbons³⁶. It is natural to raise the question of how this magnetic modulation effect on electronic and optical properties of nanoribbons evolves with varying parameter α in the $\alpha - T_3$ lattice.

In this work, we investigate systematically the magnetic modulation effect on electronic and optical properties of nanoribbons made from the $\alpha - T_3$ lattice. We show that the magnetic field can open a gap and induce an absorption peak in both the metallic armchair rib-

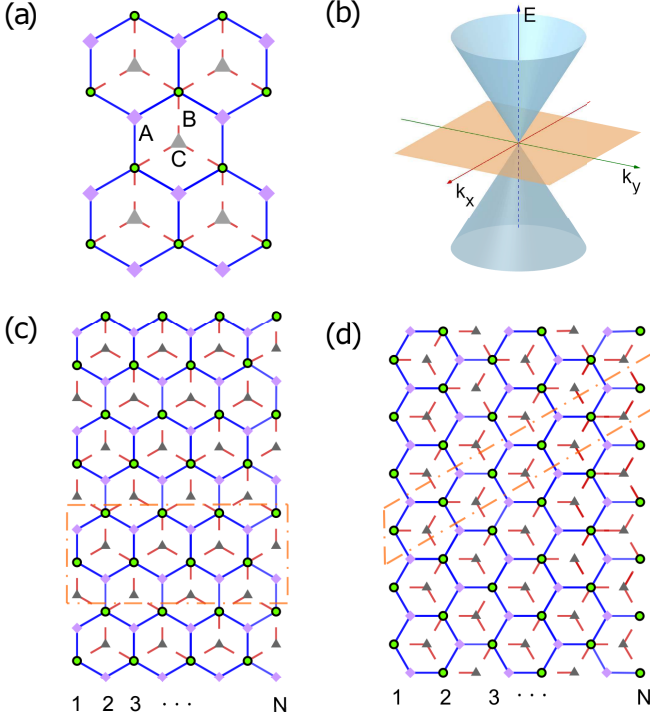


FIG. 1. (a) The lattice of the $\alpha - T_3$ model. (b) The low-energy dispersion at a single K point. (c) An armchair ribbon from the $\alpha - T_3$ lattice with the width N . (d) A B-B edged zigzag ribbon from the $\alpha - T_3$ lattice with the width N where B atoms terminates at both the left and right edges.

bons and a special type of zigzag ribbons. This magnetic modulation effect is remarkably enhanced in contrast to that in graphene due to the interband transitions between the flat band and the propagating bands, which makes the optical response much more sensitive to the applied magnetic field. We also present analytical discussions to explain this enhanced magnetic modulation effect in the $\alpha - T_3$ lattice. Without the magnetic field, the low frequency conductivity is usually zero and the first response peak appears at a frequency corresponding to the allowed transition with the lowest energy gap. We show that the large threshold frequency that prevented terahertz and far-infrared (FIR) response in ribbons can be reduced to a much lower value by a magnetic field, making these ribbons active in the terahertz and FIR regime. The applied magnetic field is much weaker than that needed in graphene. Therefore controlled terahertz radiation can be achieved much more easily in nanoribbons made from the $\alpha - T_3$ lattice through the applied magnetic field.

The rest of the paper is organized as follows. In Sec. II, we present the model and the Kubo formula for the calculation of the optical conductivity. The numerical results and discussions on electronic structure and optical conductivity will be presented for armchair ribbons in Sec. III, and for zigzag ribbons in Sec. IV. Finally, conclusion remarks are given in Sec. V.

II. MODEL AND KUBO FORMULA

In the $\alpha - T_3$ lattice shown in Fig. 1(a), sites A and B form honeycomb lattice, and site C at the center of the hexagons. The hopping energy between sites A and B is $t_1 = t \cos \varphi$, and the hopping between sites B and C is $t_2 = t \sin \varphi$. The parameter α is defined as $\alpha = t_2/t_1 = \tan \varphi$. And the hopping between sites A and C is not permitted. This $\alpha - T_3$ model interpolates between the honeycomb lattice of graphene and the dice lattice via the parameter α . Under a perpendicular magnetic field, the tight-binding Hamiltonian on the basis $(\psi_A, \psi_B, \psi_C)^T$ is given by

$$H = \sum_{\langle i,j \rangle, \langle j,k \rangle} (t \cos \varphi e^{i\gamma_{ij}} a_i^\dagger b_j + t \sin \varphi e^{i\gamma_{jk}} b_j^\dagger c_k + \text{H.c.}) \quad (1)$$

where $\varphi = \arctan \alpha$, a^\dagger , b^\dagger , and c^\dagger (a , b , c) are creation (annihilation) operators at sites A, B, C respectively. Here $\gamma_{ij(jk)} = (2\pi/\phi_0) \int_{i(j)}^{j(k)} \mathbf{A} \cdot d\mathbf{l}$ is the magnetic Peierls phase, with $\phi_0 = hc/e$ being the magnetic flux quantum. The magnetic field in the z direction is described by the vector potential $\mathbf{A} = Bx\hat{y}$ in the Landau gauge. In the nanoribbon geometry shown in Figs. 1(c) and 1(d), the Hamiltonian can be constructed on the basis of the supercell from the Harper equation.

Without the magnetic field, the continuum Hamiltonian of the $\alpha - T_3$ model can be written as

$$H_0 = \begin{pmatrix} 0 & \cos \varphi f(\mathbf{k}) & 0 \\ \cos \varphi f^*(\mathbf{k}) & 0 & \sin \varphi f(\mathbf{k}) \\ 0 & \sin \varphi f^*(\mathbf{k}) & 0 \end{pmatrix}, \quad (2)$$

where $f(\mathbf{k}) = t(1 + e^{-i\mathbf{k} \cdot \mathbf{a}_1} + e^{-i\mathbf{k} \cdot \mathbf{a}_2}) = |f(\mathbf{k})|e^{i\theta_k}$ with \mathbf{k} the momentum and θ_k being the complex angle of $f(\mathbf{k})$, $\mathbf{a}_1 = (-\frac{\sqrt{3}}{2}, \frac{3}{2})a$, $\mathbf{a}_2 = (\frac{\sqrt{3}}{2}, \frac{3}{2})a$. The eigenvalues can be obtained as $E_0 = 0$ and $E_\pm = \pm |f(\mathbf{k})|$. The corresponding eigenfunctions are

$$\xi_0 = \begin{pmatrix} \sin \varphi e^{i\theta_k} \\ 0 \\ -\cos \varphi e^{-i\theta_k} \end{pmatrix}, \quad \xi_\pm = \frac{1}{\sqrt{2}} \begin{pmatrix} \cos \varphi e^{i\theta_k} \\ \pm 1 \\ \sin \varphi e^{-i\theta_k} \end{pmatrix} \quad (3)$$

with the ξ_0 denoting the flat band, ξ_\pm denoting the conduction (+) and valence (-) bands. The full wave function reads $\psi = \xi e^{i(k_x x + k_y y)}$.

To consider nanoribbons, we construct the Harper equation from the lattice Hamiltonian. For armchair ribbons, the Harper equation reads

$$E\psi_m = B_{m-1}\psi_{m-1} + D_m\psi_m + B_m\psi_{m+1} \quad (4)$$

where m is the cell index in a supercell as shown in Fig. 1(c), $\psi_m = (\psi_{Am} \ \psi_{Bm} \ \psi_{Cm})^T$. On the basis $\psi = (\psi_1 \ \psi_2 \ \psi_3 \ \cdots \ \psi_N)^T$, we can construct the Hamiltonian of an armchair nanoribbon with width N as fol-

lows

$$H_{arm} = \begin{pmatrix} D_1 & B_1 & 0 & \cdots & 0 \\ B_1 & D_2 & B_2 & \cdots & 0 \\ 0 & B_2 & D_3 & \cdots & 0 \\ \cdots & \cdots & \cdots & \cdots & \cdots \\ 0 & 0 & 0 & \cdots & D_N \end{pmatrix}, \quad (5)$$

where

$$B_m = \begin{pmatrix} 0 & \cos \varphi g_{1m} & 0 \\ \cos \varphi g_{1m}^* & 0 & \sin \varphi g_{1m} \\ 0 & \sin \varphi g_{1m}^* & 0 \end{pmatrix}, \quad (6)$$

$$D_m = \begin{pmatrix} 0 & \cos \varphi g_{2m} & 0 \\ \cos \varphi g_{2m}^* & 0 & \sin \varphi g_{2m} \\ 0 & \sin \varphi g_{2m}^* & 0 \end{pmatrix}. \quad (7)$$

Here $g_{1m} = t \exp[i\frac{\pi}{3}f(m' + \frac{1}{2}) + \frac{a}{2}k_y]$ and $g_{2m} = t \exp[-i(\frac{2}{3}\pi f m' + k_y a)]$, with $m' = m - (N + 1)/2$ and $f = 3\sqrt{3}Ba^2/2\phi_0$ being the magnetic flux through the hexagon in units of ϕ_0 . a is the bond length and k_y is the wave vector along the y direction due to the preserved translational symmetry. Note that we use the replacement $m' = m - (N + 1)/2$ to display the reflection symmetry of the system. And the physical width of an armchair ribbon with width notation N is $W = \sqrt{3}a(N - 1)/2$.

For zigzag ribbons as shown in Fig. 1(d), the Harper equation reads

$$E\psi_m = A_{m-1}^\dagger \psi_{m-1} + C_m \psi_m + A_m \psi_{m+1}. \quad (8)$$

The Hamiltonian of a zigzag ribbon with width N is given by

$$H_{zz} = \begin{pmatrix} C_1 & A_1 & 0 & \cdots & 0 \\ A_1^\dagger & C_2 & A_2 & \cdots & 0 \\ 0 & A_2^\dagger & C_3 & \cdots & 0 \\ \cdots & \cdots & \cdots & \cdots & \cdots \\ 0 & 0 & 0 & \cdots & C_N \end{pmatrix}, \quad (9)$$

where

$$A_m = \begin{pmatrix} 0 & t \cos \varphi & 0 \\ 0 & 0 & t \sin \varphi \\ 0 & 0 & 0 \end{pmatrix}, \quad (10)$$

$$C_m = \begin{pmatrix} 0 & \cos \varphi g_{3m+} & 0 \\ \cos \varphi g_{3m+}^* & 0 & \sin \varphi g_{3m-} \\ 0 & \sin \varphi g_{3m-}^* & 0 \end{pmatrix}, \quad (11)$$

with $g_{3m\pm} = 2t \cos[\pi f(m' \pm \frac{1}{6}) + \frac{\sqrt{3}a}{2}k_y]$. And the physical width of a zigzag ribbon with width N is $W = 3aN/2 - a/2$. For zigzag ribbons, there are three types of situations for both the left and right boundary according to the termination atom, A edged, B edged, and C edged boundaries, respectively. The submatrices C_1 , A_1 , C_N , and A_{N-1} should be modified to fit two particular boundaries of the ribbon. The method is straightforward and the details are not shown here for space limitation.

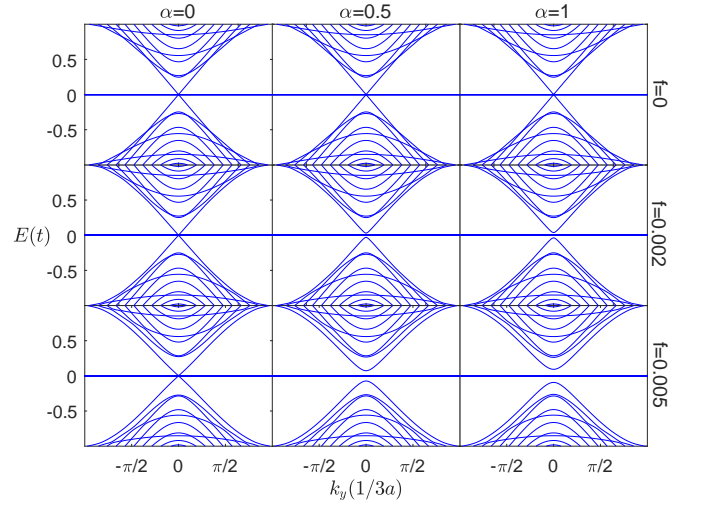


FIG. 2. Band structures of metallic armchair ribbons with various $\alpha = 0, 0.5, 1$ and magnetic flux $f = 0, 0.002, 0.005$. The width of the ribbon is fixed to $N = 20$.

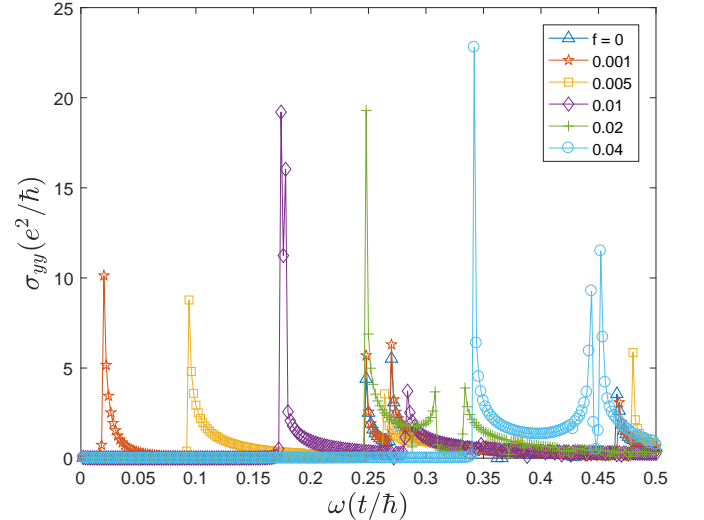


FIG. 3. Optical conductivity of a metallic armchair ribbon under various magnetic field. The parameters are $N = 20$, $\alpha = 1$, the chemical potential $\mu = 0$, the temperature $T = 300K$, and $\delta = 10^{-4}t$.

By diagonalizing the Hamiltonian, we can obtain all the eigenvalues ϵ_{kj} and corresponding eigenfunctions $\psi_{kj} = \phi_j e^{iky}$, where ϕ_j denotes the j th eigenvector of the Hamiltonian matrix for a fixed $k_y = k$, with $j = 1, 2, 3 \dots 3N$. In order to calculate the optical conductivity of ribbons using the Kubo formula, we first write the form of the current operator along the longitudinal direction $J_y = e \frac{\partial H}{\hbar \partial k_y}$. By introducing the field operator $\hat{\psi}(x, y) = \sum_{kj} \phi_j e^{iky} c_{kj}$ with c_{kj} being the annihilation operator in state ψ_{kj} , the current operator can be expressed in the second quantization notation,

$\hat{J}_y = \sum_{k_{jj'}} J_{jj'}^y c_{k_j}^\dagger c_{k_{j'}}$, with $J_{jj'}^y = \phi_j^\dagger J_y \phi_{j'}$. According to the Kubo formula, the optical conductivity is found as

$$\sigma_{yy}(\omega) = -\frac{1}{i\omega W} \sum_{k_{jj'}} \frac{J_{jj'}^y(k) J_{j'j}^y(k) (f_{k_j} - f_{k_{j'}})}{\hbar\omega + \epsilon_{k_j} - \epsilon_{k_{j'}} + i\delta}, \quad (12)$$

where f_{k_j} is the Fermi distribution function, δ is a positive infinitesimal, and W is the physical width of the ribbon.

III. ARMCHAIR RIBBONS

A. Numerical results

Fig. 2 shows the evolution of the band structure of a metallic armchair ribbon with various parameter α under various magnetic field. The width of the ribbon is $N = 20$, which satisfies the condition $N = 3n - 1$ of the metallic armchair ribbons. When the magnetic field is absent, the band structure is gapless for arbitrary α . Under a magnetic field, the band structure opens a gap, but the flat band remains untouched. For $\alpha = 0$ (graphene), the gap is very tiny. With increasing α , the gap is increasing and remarkably enhanced for even modest α .

Fig. 3 plots the optical conductivity of a metallic armchair ribbon under various magnetic field. The ribbon is made from the dice lattice ($\alpha = 1$) and the width is $N = 20$. Without the magnetic field, the flat band and two linear subbands cross at zero energy, and the spectrum is almost the same as in graphene. The first absorption peak appears at a frequency $0.25t/\hbar$ which corresponds to the transition between the flat band and the first parabolic subband. When the magnetic field is present, there opens a gap in the band structure. The numerical results show that the first response peak in the optical conductivity has the frequency which corresponds exactly to the opened gap. This absorption peak is attributed to the transitions between the flat band and two gapped subbands. The gap opening remarkably reduces the threshold frequency. For $f = 0.001$, the threshold frequency is reduced to $0.02t/\hbar$. It is noted that the gap and the threshold frequency can be continuously tuned by the magnetic field. By comparison with the earlier results for graphene without the flat band^{36,44}, it is clearly shown that the magnetic modulation effect on the optical response is significantly enhanced.

For armchair ribbons with width $N \neq 3n - 1$, there is a gap in the band structure due to the discreteness of k_x . Applying a weak magnetic field only modifies slightly the gap and shifts the first absorption peak weakly. For comparison with graphene, $t = 3$ eV and $a = 1.42$ Å are used in all the calculations. The corresponding magnetic field is nearly 78 T for the magnetic flux $f = 0.001$. For a realistic $\alpha - T_3$ material with much larger lattice constant, this corresponding magnetic field can be much reduced. Moreover, it is noticeable that even a very weak magnetic field can open a gap and induce an absorption

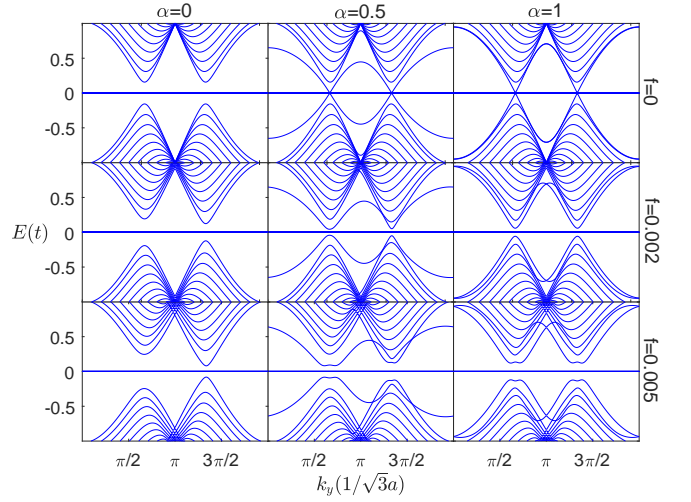


FIG. 4. Band structures of B-B edged zigzag ribbons with various $\alpha = 0, 0.5, 1$ and magnetic flux $f = 0, 0.002, 0.005$. The width of the ribbon is fixed to $N = 20$.

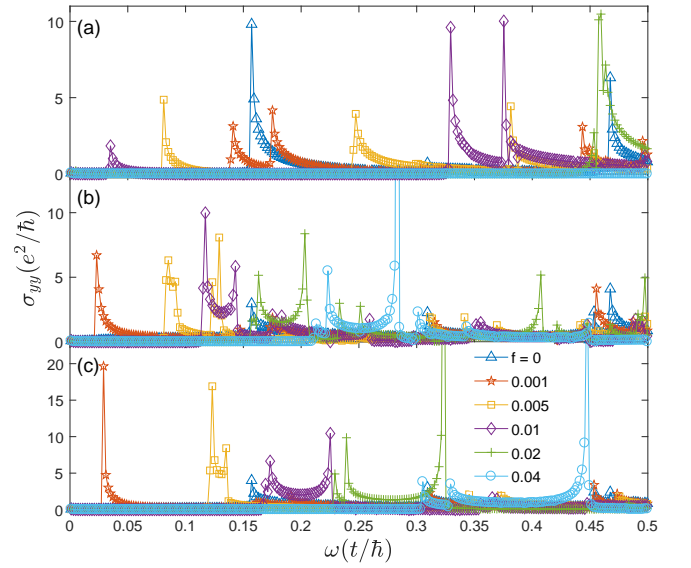


FIG. 5. Optical conductivity of a B-B edged zigzag ribbon under various magnetic field for different parameter α : (a) $\alpha = 0$, (b) $\alpha = 0.5$, (c) $\alpha = 1$. The other parameters are $N = 20$, $\mu = 0$, $T = 300K$, and $\delta = 10^{-4}t$.

peak, but with a very low frequency. The room temperature $T = 300K$ is used in all the calculations of optical conductivities. Fig. 3 shows that the new absorption peak for $f = 0.001$ is still sharp even at room temperature. For smaller magnetic field, the new absorption peak with lower frequency may be broaden at high temperature. But we argue that the temperature only affects the width of absorption peaks, not the position of them.

B. Analytic discussions

To better understand the magnetic modulation effect on the optical response in armchair ribbons made from the $\alpha - T_3$ lattice, we analytically investigate the gap opening mechanism in the presence of a weak magnetic field.

The spectrum of armchair ribbons can be obtained by imposing proper boundary conditions to the wave functions sloved from the continuum Hamiltonian (Eq. (2)). For an armchair ribbon with width N , the boundary conditions become $\psi(x=0) = \psi[x = \frac{\sqrt{3}a}{2}(N+1)] = 0$. Therefore the transverse momentum k_x has to take discrete values as

$$k_x = \frac{j\pi}{\frac{\sqrt{3}a}{2}(N+1)} = \frac{2\pi}{\sqrt{3}a} \frac{l}{N+1}, \quad (13)$$

where $l = 1, 2, 3, \dots, N$ is the subband index. For the l th subband, the wave function is

$$\psi_j = \sqrt{\frac{2}{N+1}} \xi \sin \frac{lm\pi}{N+1} e^{ik_y y} \quad (14)$$

with $m = 1, 2, 3, \dots, N$ being the site position along the x direction. When $N = 3n - 1$, the $2n$ th subband with $k_x = \frac{4\pi}{3\sqrt{3}a}$ sweeps through the Dirac point $(\frac{4\pi}{3\sqrt{3}a}, 0)$, which makes the ribbon metallic. We focus on only the flat band $|l0\rangle$ (containing N subbands, $l = 1, 2, 3, \dots, N$), the $2n$ th conduction band $|2n+\rangle$, and the $2n$ th valence band $|2n-\rangle$. These subbands cross at zero energy at $k_y = 0$ for metallic armchair ribbons, and are crucial to the gap opening under a magnetic field.

We consider a weak magnetic field as a perturbation. To obtain the perturbation Hamiltonian, we first linearize $f(\mathbf{k})$ around the Dirac point $\mathbf{K} = (\frac{4\pi}{3\sqrt{3}a}, 0)$ as $f(\mathbf{k}) \rightarrow \hbar v_F(-k_x + ik_y)$, where $v_F = \frac{3at}{2\hbar}$ is the Fermi velocity and k_x and k_y are measured from the \mathbf{K} point from now on. And now $\theta_k = \arctan(k_y/k_x)$ becomes the momentum direction angle. Under a magnetic field, k_y should be replaced by $k_y + eA_y/\hbar c$ with $A_y = Bx$. Then the perturbation Hamiltonian of the magnetic field reads

$$H_1 = \pi t f m' \begin{pmatrix} 0 & i \cos \varphi & 0 \\ -i \cos \varphi & 0 & i \sin \varphi \\ 0 & -i \sin \varphi & 0 \end{pmatrix} \quad (15)$$

where $m' = m - \frac{N+1}{2}$. Here we reset the midpoint of the ribbon as the zero point in the x axis. Now we calculate the magnetic field induced couplings among $|j0\rangle$, $|2n+\rangle$,

and $|2n-\rangle$ as follows

$$\begin{aligned} \langle 2n\pm | H_1 | 2n\pm \rangle &= \pm \pi t f \sin \theta_k \sum_m m' \sin^2 \left(\frac{2\pi}{3} m \right) \approx 0, \\ \langle 2n\mp | H_1 | 2n\pm \rangle &= \pm i \pi t f \cos \theta_k \cos 2\varphi \sum_m m' \sin^2 \left(\frac{2\pi}{3} m \right) \\ &= 0, \\ \langle l0 | H_1 | 2n\pm \rangle &= \pm \frac{i}{\sqrt{2}} \pi t f \cos \theta_{kl} \sin 2\varphi \\ &\quad \cdot \sum_m m' \sin \left(\frac{l\pi}{N+1} m \right) \sin \left(\frac{2\pi}{3} m \right) \\ &\approx \begin{cases} \mp i \pi t f \cos \theta_{kl} \sin 2\varphi \frac{8nl(N+1)^2}{\pi^2(l^2 - 4n^2)^2}, & l \text{ is odd} \\ 0, & l \text{ is even} \end{cases} \\ \langle l0 | H_1 | l'0 \rangle &= 0, \end{aligned} \quad (16)$$

where θ_k (θ_{kl}) is the momentum direction angle of the state $|2n\pm\rangle$ ($|l0\rangle$). From the above matrix elements, we can see that the gap opening is attributed to the coupling between the flat band $|l0\rangle$ and two linear subbands $|2n\pm\rangle$. And the factor $\sin 2\varphi$ shows that this coupling vanishes for graphene ($\alpha = 0$). The gap opening in graphene is attributed to the coupling between two linear subbands and other parabolic subbands with higher energies. The energy difference between them makes the perturbation correction in energy very tiny. The opened gap leads to the first response peak which is fully tunable by the magnetic field.

IV. ZIGZAG RIBBONS

A. B-B edged zigzag ribbons

For zigzag ribbons, there are three types of boundaries for both two edges, namely, A edged, B edged, and C edged boundaries, respectively. We find that only in B-B edged zigzag ribbons can the magnetic field open a gap and give rise to a new absorption peak. Fig. 4 shows the band structure of the B-B edged zigzag ribbon with various α and magnetic field. When $\alpha = 0$ and $f = 0$, the spectrum is gaped due to the quantum confinement effect. The flat band and the zigzag edge state subbands are degenerate at zero energy and go through the whole Brillouin zone. With nonzero α , two zigzag edge state subbands become linearly dispersive subbands and cross each other at two Dirac points. When the magnetic field is applied, the coupling between the flat band and two linear subbands opens a gap, which is similar to the situation in metallic armchair ribbons. It is also worthy to note that the valley degeneracy of the band structure is lifted by the magnetic field in the case of $\alpha < 1$, which will lead to the splitting of response peaks.

The corresponding optical conductivities are plotted in Fig. 5. When $\alpha = 0$ and $f = 0$, the spectrum is gapped and the first absorption peak is due to the transition between zero-energy edge states and the first parabolic

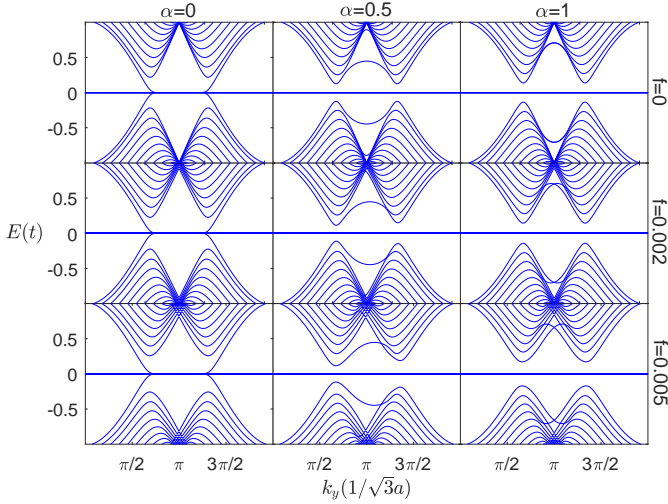


FIG. 6. Band structures of C-A edged zigzag ribbons with various $\alpha = 0, 0.5, 1$ and magnetic flux $f = 0, 0.002, 0.005$. The width of the ribbon is fixed to $N = 20$.

subband. When the magnetic field is tuned on, the peak is splitted. With increasing magnetic field, the splitting is larger. However, the situation is quite different in the case of $\alpha > 0$. In these cases, the zero-energy edge states evolve into two linearly dispersive subbands around the Dirac points. But the first absorption peak changes little because it still corresponds to the transition between the flat band to the first parabolic subband. When the magnetic field is applied, two linear subbands open a gap. The transitions between the flat band and two gapped subbands give rise to a new absorption peak with much reduced frequency, as shown in Figs. 5(b) and 5(c).

B. C-A edged zigzag ribbons

For zigzag ribbons with other boundaries, the applied magnetic field can not give rise to a new absorption peak. Because the situation is similar for all these zigzag ribbons, we take C-A edged zigzag ribbon as an example to present the results.

Fig. 6 shows the band structure of the C-A edged zigzag ribbon with various α and magnetic field. When $\alpha = 0$ and $f = 0$, the spectrum is gapless because the edge states continuously connect to the bulk states. With nonzero α , the edge states are gapped. An applied weak magnetic field only slightly modifies the gap, and the modification is different for two valleys when $0 < \alpha < 1$, which leads to the lifting of valley degeneracy. In the case of $\alpha = 0$, the applied magnetic field only slightly modifies the bulk subbands and the edges states remain gapless.

The corresponding optical conductivities are plotted in Fig. 7. For $\alpha = 0$, the first absorption peak is due to the transition between zero-energy edge states and the first

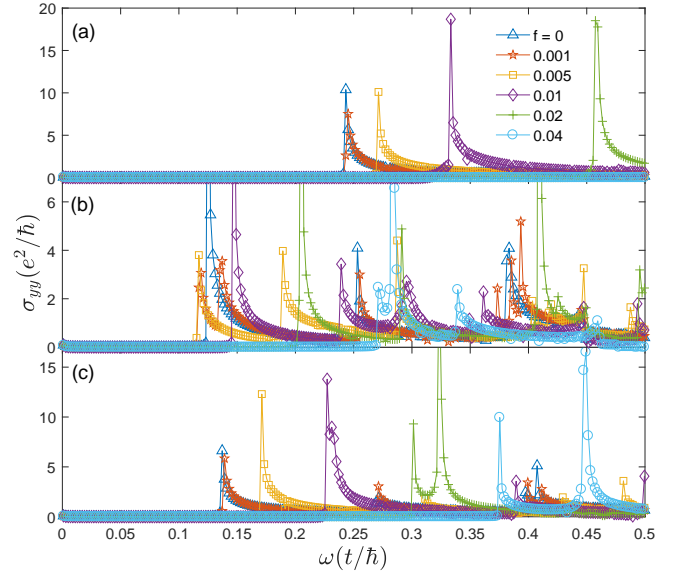


FIG. 7. Optical conductivity of a C-A edged zigzag ribbon under various magnetic field for different parameter α : (a) $\alpha = 0$, (b) $\alpha = 0.5$, (c) $\alpha = 1$. The other parameters are $N = 20$, $\mu = 0$, $T = 300K$, and $\delta = 10^{-4}t$.

parabolic subband. The applied weak magnetic field only slightly shifts the first peak. With increasing magnetic field, the shifting is larger. For nonzero α , the edge states are gapped and the first absorption peak emerges due to the transition between the flat band and the newly gapped edge states. When $\alpha = 1$, the valley degeneracy is preserved and the magnetic field only shifts the first peak. But when $0 < \alpha < 1$, the valley degeneracy is lifted and then the magnetic field splits the first absorption peak. Overall, the magnetic field can not give rise to a new absorption peak in zigzag ribbons where the two boundaries are not B-B edged.

V. CONCLUSION

In conclusion, we investigated the influence of a weak magnetic field on the band structure and magneto-optical properties of nanoribbons made from the $\alpha - T_3$ lattice. It is found that the magnetic field can open a gap in the band structure and induces a new absorption peak with much reduced frequency in metallic armchair ribbons and B-B edged zigzag ribbons. The flat band plays a key role in the gap opening and the emergence of a new absorption peak in the optical conductivity. And this magneto-optical modulation effect is much stronger than that in metallic armchair graphene ribbons due to the presence of the flat band. We explained the enhancement of the optical response under a magnetic field within the perturbation theory for metallic armchair ribbons. And the situation is similar in B-B edged zigzag ribbons. For the applications in magneto-optics devices, the applied mag-

netic field is much weaker than that needed in graphene. Therefore controlled terahertz radiation can be achieved much more easily in nanoribbons made from the $\alpha - T_3$ lattice. Besides, we also find the magnetic field will lift the valley degeneracy and split the absorption peaks in zigzag ribbons. We propose that this enhanced magneto-optical response may be observable in the quantum wire of critically doped $\text{Hg}_{1-x}\text{Cd}_x\text{Te}$. These findings pave the way for magneto-optics devices based on the $\alpha - T_3$ model materials.

ACKNOWLEDGMENTS

The work described in this paper is supported by the National Natural Science Foundation of China (NSFC, Grant Nos. 11774144, 11774006, and 11574045), and NBRP of China (2012CB921300).

-
- * phjfiu@gzhu.edu.cn
† mazs@pku.edu.cn
- ¹ A. H. Castro Neto, F. Guinea, N. M. R. Peres, K. S. Novoselov, and A. K. Geim, *Rev. Mod. Phys.* **81**, 109 (2009).
 - ² N. M. R. Peres, *Rev. Mod. Phys.* **82**, 2673 (2010).
 - ³ S. Das Sarma, Shaffique Adam, E. H. Hwang, and Enrico Rossi, *Rev. Mod. Phys.* **83**, 407 (2011).
 - ⁴ J. Vidal, R. Mosseri, and B. Douçot, *Phys. Rev. Lett.* **81**, 5888 (1998).
 - ⁵ J. Vidal, P. Butaud, B. Douçot, and R. Mosseri, *Phys. Rev. B* **64**, 155306 (2001).
 - ⁶ B. Dóra, J. Kailasvuori, and R. Moessner, *Phys. Rev. B* **84**, 195422 (2011).
 - ⁷ F. Wang and Y. Ran, *Phys. Rev. B* **84**, 241103 (2011).
 - ⁸ D. Bercioux, D. F. Urban, H. Grabert, and W. Häusler, *Phys. Rev. A* **80**, 063603 (2009).
 - ⁹ J. D. Malcolm and E. J. Nicol, *Phys. Rev. B* **92**, 035118 (2015).
 - ¹⁰ F. Piéchon, J.-N. Fuchs, A. Raoux, and G. Montambaux, *Journal of Physics: Conference Series* **603**, 012001 (2015).
 - ¹¹ J. D. Malcolm and E. J. Nicol, *Phys. Rev. B* **90**, 035405 (2014).
 - ¹² Z. Lan, N. Goldman, A. Bermudez, W. Lu, and P. Öhberg, *Phys. Rev. B* **84**, 165115 (2011).
 - ¹³ A. Raoux, M. Morigi, J.-N. Fuchs, F. Piéchon, and G. Montambaux, *Phys. Rev. Lett.* **112**, 026402 (2014).
 - ¹⁴ T. Louvet, P. Delpierre, A. A. Fedorenko, and D. Carpentier, *Phys. Rev. B* **92**, 155116 (2015).
 - ¹⁵ Di Xiao, Ming-Che Chang, and Qian Niu, *Rev. Mod. Phys.* **82**, 1959–2007 (2010).
 - ¹⁶ Yong Xu and L.-M. Duan, *Phys. Rev. B* **96**, 155301 (2017).
 - ¹⁷ Tutul Biswas and Tarun Kanti Ghosh, *J. Phys.: Condens. Matter* **28**, 495302 (2016).
 - ¹⁸ Daniel F. Urban, Dario Bercioux, Michael Wimmer, and Wolfgang Häusler, *Phys. Rev. B* **84**, 115136 (2011).
 - ¹⁹ R. Shen, L. B. Shao, Baigeng Wang, and D. Y. Xing, *Phys. Rev. B* **81**, 041410 (2010).
 - ²⁰ E. Illes and E. J. Nicol, *Phys. Rev. B* **95**, 235432 (2017).
 - ²¹ Y. Betancur-Ocampo, G. Cordourier-Maruri, V. Gupta, and R. de Coss, *Phys. Rev. B* **96**, 024304 (2017).
 - ²² SK Firoz Islam and Paramita Dutta, *Phys. Rev. B* **96**, 045418 (2017).
 - ²³ Máté Vigh, László Oroszlány, Szabolcs Vajna, Pablo San-Jose, Gyula Dávid, József Cserti, and Balázs Dóra, *Phys. Rev. B* **88**, 161413(R) (2013).
 - ²⁴ Cheng-Zhen Wang, Hong-Ya Xu, Liang Huang, and Ying-Cheng Lai, *Phys. Rev. B* **96**, 115440 (2017).
 - ²⁵ Z. Liu, Z.-F. Wang, J.-W. Mei, Y.-S. Wu, and F. Liu, *Phys. Rev. Lett.* **110**, 106804 (2013).
 - ²⁶ M. G. Yamada, T. Soejima, N. Tsuji, D. Hirai, M. Dincă, and H. Aoki, *Phys. Rev. B* **94**, 081102 (2016).
 - ²⁷ Ninghai Su, Wei Jiang, Zhengfei Wang, and Feng Liu, *Appl. Phys. Lett.* **112**, 033301 (2018).
 - ²⁸ Sebastiano Peotta and Päivi Törmä, *Nat. Commun.* **6**, 8944 (2015).
 - ²⁹ E. Tang, J.-W. Mei, and X.-G. Wen, *Phys. Rev. Lett.* **106**, 236802 (2011).
 - ³⁰ Kai Sun, Zhengcheng Gu, Hosho Katsura, and S. Das Sarma, *Phys. Rev. Lett.* **106**, 236803 (2011).
 - ³¹ T. Neupert, L. Santos, C. Chamon, and C. Mudry, *Phys. Rev. Lett.* **106**, 236804 (2011).
 - ³² Z. F. Wang and Feng Liu, *Appl. Phys. Lett.* **99**, 042110 (2011).
 - ³³ Chao Zhang, Lei Chen, and Zhongshui Ma, *Phys. Rev. B* **77**, 241402(R) (2008).
 - ³⁴ D. Prezzi, D. Varsano, A. Ruini, A. Marini, and E. Molinari, *Phys. Rev. B* **77**, 041404(R) (2008).
 - ³⁵ H. Hsu and L. E. Reichl, *Phys. Rev. B* **76**, 045418 (2007).
 - ³⁶ Junfeng Liu, A. R. Wright, Chao Zhang, and Zhongshui Ma, *Appl. Phys. Lett.* **93**, 041106 (2008).
 - ³⁷ A. R. Wright, J. C. Cao, and C. Zhang, *Phys. Rev. Lett.* **103**, 207401 (2009).
 - ³⁸ Wenhui Liao, Guanghui Zhou, and Fu Xi, *J. Appl. Phys.* **104**, 126105 (2008).
 - ³⁹ Xin-Xiang Peng, Wen-Hu Liao, and Guang-Hui Zhou, *Chin. Phys. Lett.* **25**, 3436 (2008).
 - ⁴⁰ Jonas Have and Thomas G. Pedersen, *Phys. Rev. B* **97**, 115405 (2018).
 - ⁴¹ E. Illes, J. P. Carbotte, and E. J. Nicol, *Phys. Rev. B* **92**, 245410 (2015).
 - ⁴² E. Illes and E. J. Nicol, *Phys. Rev. B* **94**, 125435 (2016).
 - ⁴³ Áron Dániel Kovács, Gyula Dávid, Balázs Dóra, and József Cserti, *Phys. Rev. B* **95**, 035414 (2017).
 - ⁴⁴ C. Vacacela Gomez, M. Pizarra, M. Gravina, J. M. Pitarke, and A. Sindona, *Phys. Rev. Lett.* **117**, 116801 (2016).